Industrial Crops & Products 145 (2020) 112105

Contents lists available at ScienceDirect

Industrial Crops & Products

journal homepage: www.elsevier.com/locate/indcrop

Pure, stable and highly antioxidant lignin nanoparticles from elephant grass

Henrique Trevisan, Camila A. Rezende*

Institute of Chemistry, University of Campinas, PO Box 6154, 13083-970, Campinas, SP, Brazil

ARTICLE INFO

Keywords:
Lignin nanoparticle
Biomass
Pretreatment
Acid-alkali
DPPH test
Elephant grass

ABSTRACT

Finding renewable and green resources for nanomaterial preparation is a compelling topic concerning the sustainability in nanotechnological applications. In particular, lignin-based nanoparticles are pivotal for unlocking the use of lignin in value added products. In this paper, we isolated pure lignin (ca. 98 % of purity) from elephant grass (*Pennisetum purpureum*) using two simple extractions with diluted acid and alkali solutions and prepared lignin and lignin acetate nanoparticles dispersed in water-basis by anti-solvent addition. Elephant grass in natura contains ca. 25 % of lignin, which could be converted into lignin nanoparticles with a 37 % yield. Spherical lignin and lignin acetate nanoparticles were revealed by electron microscopies (TEM and FESEM) and proved to be stable in a wide pH range (5–11) and ionic strength lower than 0.01. Lignin nanoparticles showed higher antioxidant activity (RSI of ca. 82) as compared to lignin in solution and to the commercial antioxidants (BHT and BHA). These nanoparticles were successfully incorporated in a neutral cream, resulting in a tinted sunscreen formulation with both ultraviolet and visible absorption. Altogether, we present here an effective method to isolate pure lignin from a non-food biomass and to prepare stable and highly antioxidant lignin nanoparticles that can be applied in dermocosmetics and are intrinsically non-toxic to the environment.

1. Introduction

Lignin is an important biomacromolecule that contains key phenylpropanoid structures for the production of greener chemicals and lignin-based materials (Ragauskas et al., 2014). In spite of its attractive physicochemical properties, such as resistance to oxidation, UV radiation absorption, antioxidant and bactericidal activities, this biomacromolecule is still underutilized in comparison to other components from lignocellulosic biomass (Fang and Smith, 2016; Ragauskas et al., 2014; Strassberger et al., 2014; Yang et al., 2018a, 2018b; Zhao et al., 2016). Among the potential renewable sources for lignin isolation, those derived from non-food lignocellulosic biomasses have been receiving great attention, together with lignin recovery during the extraction of cellulose in paper industry (Figueiredo et al., 2018).

Elephant grass is a promising biomass for this purpose, since it has high lignin content (22–28 wt.%), high productivity per hectare (ca. 50 tons ha^{-1} y^{-1}), low demand for nutrients and high resistance to harsh climates (Lima et al., 2014; Menegol et al., 2017; Nascimento and Rezende, 2018; Somerville et al., 2010). It is also a plant that intakes large amounts of CO_2 from the environment (ca. 15 tons of carbon ha^{-1} y^{-1}), which is a beneficial aspect in terms of carbon cycle (Nascimento and Rezende, 2018). Favourably, recent studies showed that this perennial grass have great potential for cellulosic ethanol production, from which lignin would be an important by-product (Rezende et al., 2018; Somerville et al., 2010).

Different methods have been reported for lignin isolation from plant biomasses, among which are worth mentioning: 1. Kraft, 2. Sulphite, 3. Soda (alkali) and 4. Organosolv (Figueiredo et al., 2018; Schutyser et al., 2018). The Kraft and the sulphite methods are considered to be pollutant and they result in lignins containing high amounts of sulphur (Kai et al., 2016). Soda and organosolv treatments, on the other hand, allow the extraction of lignin without the insertion of sulphur in its structure (Ahvazi et al., 2016; Figueiredo et al., 2018). Organosolv methods may lead to lignin with high purity (values from ca. 70–90 wt. %), but they depend on the use of organic solvents. In turn, soda lignins are typically contaminated with high contents of carbohydrates (ca. 30 %), since the alkali treatment also removes hemicellulose, extractives and inorganic components that are transferred to the black liquor together with lignin (Florian et al., 2019; Nitsos et al., 2016). Thus, seeking a purer lignin to be converted in nanoparticles, we put forward in this work an effective and greener two-step extraction, using diluted acid and alkali solutions, which leads to hemicellulose and extractives

Abbreviations: LNP, lignin nanoparticle; AcLNP, acetylated lignin nanoparticle; DPPH, 2,2-diphenyl-1-picrylhydrazyl; RSI, radical scavenging index; BHT, butylhydroxytoluene; BHA, butylated hydroxyanisole

* Corresponding author.
E-mail address: camila@iqm.unicamp.br (C.A. Rezende).

https://doi.org/10.1016/j.indcrop.2020.112105
Received 17 July 2019; Received in revised form 5 January 2020; Accepted 7 January 2020

removal prior to the isolation of lignin.

Among the possible applications for lignin, a few recent works reported the preparation of lignin nanoparticles (Figueiredo et al., 2018; Zhao et al., 2016). In sight of its high surface-to-volume ratio, nanolignin have promising surface aspects that can lead, for instance, to improved antioxidant properties (Yang et al., 2018, 2018a; Yang et al., 2016). This is an interesting facet for dermocosmetic industries, where natural products with radical scavenging ability (essential oils, for instance) have been receiving notorious attention (Alonso et al., 2013). These antioxidant compounds are mainly phenolic terpenoids and phenylpropanoids, whose radical scavenging activity comes from the ability of phenolic groups to hinder the oxidation chain reaction (Amorati et al., 2013). Lignin, by its turn, is a potential natural antioxidant since it is constituted of phenylpropanoids and can be isolated from plants more easily and in higher amounts as compared to essential oils.

Several inorganic nanoparticles, such as gold, silver and metal oxide nanoparticles also have intrinsic antioxidant properties (Valgimigli et al., 2018). However, the environmental impact of their long-term use have been questioned, particularly concerning their persistency in waste-water treatment plants (Duan et al., 2015; Jeong et al., 2014). This problem can be mitigated by applying biodegradable nanoparticles, such as lignin, at the early stage design of nanomaterials for applications in pharmaceuticals and dermocosmetics (Kai et al., 2016). Nonetheless, studies to obtain and characterize lignin nanoparticles are quite recent with only a few reports in the literature so far (Figueiredo et al., 2018).

Here, we present a simple and effective methodology for isolation of pure lignin (ca. 98 % of purity) from a non-food biomass resource and the characterization of its key structural features after the fractionation process. Then, lignin and acetylated lignin nanoparticles were prepared by self-assembling, which were stably dispersed in water-basis in a large range of pH and ionic strength. These lignin nanoparticles also showed antioxidant activity about 1.5 times higher than lignin in solution, and 3–4 times higher than BHT and BHA, respectively, indicating their potential applicability as active antioxidant materials in dermocosmetics products.

2. Experimental Section

2.1. Materials

Elephant grass (*Pennisetum purpureum*, Guaçu cultivar) was provided by the Institute of Animal Science in Nova Odessa (SP, Brazil). The leaves were harvested one year after planting and dried in a convection oven (Tecnal TE-394/3) at 60 °C for 24 h, then knife milled through a 2 mm sieve and stored in plastic containers. The reactants used were: H_2SO_4 (98 %) and HCl (38 %) from LSChemicals; NaOH (P.A.), NaCl (P.A.), acetone (P.A.), 1,4-dioxane (P.A.), methanol (P.A.) and acetic anhydride (97 %) from Synth®; pyridine (99 %), *p*-nitrobenzaldehyde (99 %), $CDCl_3$ (100 %), DMSO-d6 (100 %), acetyl bromide (99 %), glacial acetic acid (99 %) hydroxylamine-HCl (99 %) and 2,2-diphenyl-1-picrylhydrazyl from SigmaAldrich®. A neutral aqueous base cream (DERMABASE, Dermavita) was used for the preparation of sunscreens, and commercial sunscreens with FPS 30 (Vichy Laboratories® and La Roche-Posay®) were used for comparison.

2.2. Elephant grass acid-alkali treatment for lignin isolation

The acid-alkali treatment was carried out in two steps, as previously reported by Rezende et al. in their works aiming at cellulose isolation (Nascimento and Rezende, 2018; Rezende et al., 2011). Briefly, elephant grass leaves were pretreated with aqueous H_2SO_4 1 % (v/v) in autoclave at 121 °C and 1.05 bar for 1 h applying a fixed 1:10 (g/mL) solid to solution ratio (Fig. 1). The combined severity factor calculated for this acid pretreatment step was 1.65 (Guo et al., 2008). Thereafter, the hydrolysed solid was separated from the acid liquor by filtration, washed to neutral pH and dried at 60 °C for 6 h. In the second step, the dried solid was submitted to an alkali treatment with 2 % (w/v) NaOH in autoclave under the same conditions of pressure, temperature and time of the acid treatment, using a 1:20 (g/mL) solid to liquid ratio (Fig. 1). The solid to liquid ratios are different in the acid (1:10) and in the alkali treatments (1:20) because a larger volume of liquid is required to wet the previously pretreated biomass. It happens because the starting material of the acid step (biomass *in natura*) is denser than the starting material of the alkali step (biomass previously pretreated with acid).

Lignin was precipitated from the black liquor by slow addition of H_2SO_4 (98 %) drops until reaching pH = 2. The suspension was then centrifuged at 5000 rpm for 10 min (Sorvall RC – 3B Refrigerated Centrifuge), and the solid lignin was washed and centrifuged until obtaining a clear supernatant. The amount of water used to rinse the solid was 4 times the volume of alkali solution used in the treatment, and further rinsing did not result in recover of more solid lignin. Finally, lignin was dried at 60 °C for 12 h for future structural characterization, lignin acetylation and nanoparticle preparation. Lignin acetylation followed a method previously described in literature, but starting from 1 g of lignin (Pan et al., 2006). The lignin acetate produced was also used for ^{1}H NMR (Proton Nuclear Magnetic Resonance) and GPC (Gel Permeation Chromatography) characterizations.

2.3. Lignin nanoparticle self-assembling induced by anti-solvent addition

Lignin nanoparticles were assembled following a procedure adapted from literature (Richter et al., 2016). Initially, a solution of lignin (or acetylated lignin) in acetone (5 mg mL^{-1}) was prepared and filtered through a 0.45 µm pore Nylon syringe filter to retain possible non-solubilized particles. Finally, Type I (MilliQ) water was rapidly poured in the lignin solution, applying a fixed 10:1 (v/v) water to lignin solution ratio. The system was then kept under magnetic stirring at 400 rpm for 10 min and the acetone was removed by rotary evaporation (40 °C and 40 mmHg of vacuum for 4 h). The yield of nanoparticles was determined gravimetrically by centrifuging (Sorvall RC 26 Plus SA-300 rotor, DuPont) the suspension at 20,000 rpm for 3 h with the ionic strength adjusted to 0.01, followed by supernatant removal and drying of the remaining solid pellet.

2.4. Lignin characterization

2.4.1. Quantitative ^{1}H NMR

Lignin functional groups (methoxyl; phenolic hydroxyls and aliphatic hydroxyls) were estimated based on their acetylated products using *p*-nitrobenzaldehyde as internal standard, following a method previously described in literature (Froass et al., 1998; Pan et al., 2006). The ^{1}H NMR was obtained using a Bruker Avance 400 MHz NMR Spectrometer with the following acquisition parameters: 20 ppm of spectra width, 130 scans and 2 s of acquisition time.

2.4.2. Fourier transform infrared spectroscopy (FTIR)

FTIR was used to investigate the formation of lignin acetate. The spectra were obtained within the 4000 to 500 cm^{-1} range in KBr pellets (FTIR Agilent Cary 660) with a 4 cm^{-1} resolution.

2.4.3. Gel permeation chromatography (GPC)

A VISCOTEK liquid chromatography system (Malvern Instruments Ltd.) was used and the molar masses were determined from the acetylated lignin product (1 mg) dissolved in 1 mL of tetrahydrofuran (THF), as already reported in the literature (Hu et al., 2012; Tolbert et al., 2014).

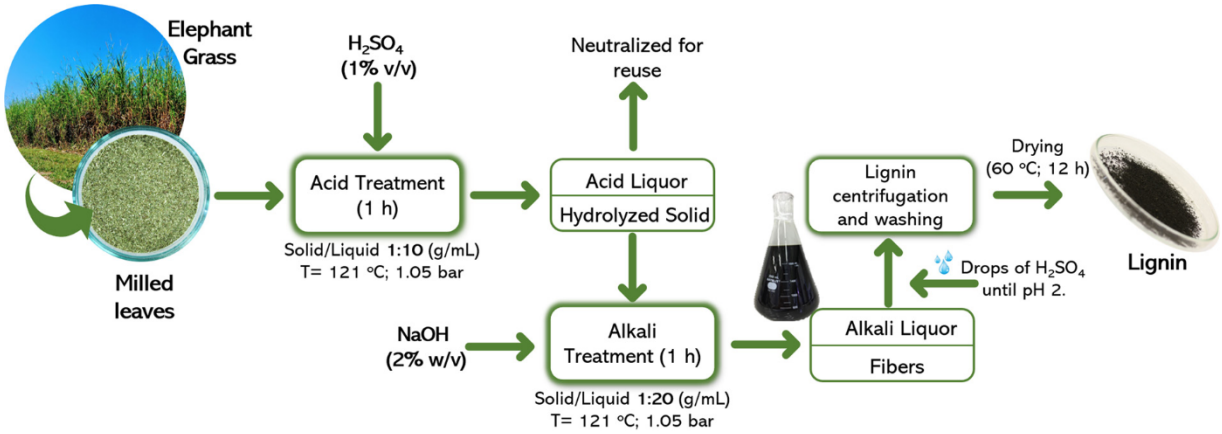

Fig. 1. Flowchart of the elephant grass acid-alkali treatment for lignin isolation and recovery.

2.4.4. Determination of lignin composition in the solids obtained after each treatment step and lignin purity

Lignin contents were firstly determined in the solid substrates using the well stablished acetyl bromide method (Moreira-Vilar et al., 2014). For so, 4 mg of solids were transferred to a 2 mL centrifuge tube, to which 250 µL of freshly prepared acetyl bromide solution (25:75 v/v acetyl bromide to glacial acetic acid) were added. After 3 h of reaction under constant stirring, the liquor was transferred to a 5 mL volumetric flask, together with 1 mL of NaOH (2 mol L^{-1}) and 175 µL of hydroxylamine-HCl (0.5 mol L^{-1}) and vortexed. Finally, the volumetric flask was filled with glacial acetic acid until the 5 mL mark and vortexed for 1 min. The lignin content was determined using a spectrophotometer from Agilent Technologies® model 8453 using a calibration curve with the absorptivity coefficient (ε) of 17.75 L g^{-1} cm^{-1}, λ = 280 nm. For determination of lignin purity, Klason lignin contents were also quantified as described in the NREL protocol (Sluiter et al., 2012).

2.5. Lignin nanoparticle characterization

2.5.1. Dynamic light scattering (DLS) and ζ-potential

A Zetasizer NANO-ZS-ZEN-3600 (Malvern Instruments Ltd.) was used in backscattering (173°) mode to obtain the mean hydrodynamic diameter and the zeta potential of the nanoparticles. The measurements were performed at 25 °C and the water viscosity was adjusted to 0.89 cP with a 1.330 refractive index. For ζ-potential measurements, a disposable folded capillary cell DTS1070 (Malvern Instruments Ltd.) was used. For the nanoparticle stability assay under variable ionic strengths, the nanoparticle suspension was diluted to 0.05 % (w/v) in NaCl solutions (1×10^{-4} to 1 mol L^{-1}). After each dilution, the mean hydrodynamic diameter and the zeta potential were measured in triplicate. For the pH stability assay, an automated titration module MPT-2 Titrator from Malvern Instruments® was used.

2.5.2. Field emission scanning electron microscopy (FESEM)

Secondary electron images were obtained in a Quanta FEG 250 (FEI) microscope operated at 5 kV. Nanoparticles were deposited on mica slides and covered with Ir, by applying a current of 11.3 mA for 90 s. A histogram of the nanoparticle size distribution was obtained by counting 500 particles in 5 different images using the ImageJ software.

2.5.3. Scanning transmission electron microscopy (STEM)

Scanning transmission images were obtained in the Quanta FEG 250 (FEI) microscope operated at 10 kV with two segment solid-state diode underneath the STEM holder. For sample preparation, nanoparticle dispersions at pH 2; 7 and 12 were pipetted (5 µL droplet) on 400 mesh copper grids (Ted Pella, Inc.), followed by drying in desiccator.

2.5.4. Transmission electron microscopy (TEM)

TEM analysis was carried out on a Carl Zeiss LIBRA 120 equipment with tungsten filament operated at 80 kV. For sample preparation, dispersions of nanoparticles were diluted to 0.05 % (w/v) and pipetted (5 µL droplet) on the copper grids followed by drying in desiccator. For TEM angular series, the sample was placed on a high tilt room temperature tomography holder (Gatan Model 916) and the equipment was operated at 120 kV. The angular series was obtained in the interval [+60, −60] degrees with step of 1 °.

2.5.5. Conductometric titration

To quantify the total amount of ionizable hydroxyl groups present on the surface of lignin nanoparticles, the suspension was titrated with NaOH 0.01 mol L^{-1} and the conductivity of the medium was monitored (conductivity meter AJX-515 from AJ Micronal®). Measurements were performed in triplicate and the concentration of ionizable groups was calculated as previously described for starch nanocrystals (Romdhane et al., 2015).

2.6. Antioxidant activity – DPPH test and UV–vis transmittance measurements

The antioxidant activities of lignin in solution and lignin nanoparticles in suspension were determined based on the colorimetric method adapted from Dizhbite et al. (2004). For the study of lignin in solution, 640 µL of lignin solution (0.001–0.5 mg mL^{-1}) in 90 % dioxane (v/v in water) were separately mixed with 2360 µL of a 65 µmol L^{-1} $DPPH^{\cdot}$ solution in methanol. For lignin nanoparticles, aqueous suspensions (0.001–0.5 mg mL^{-1}) were used instead of lignin solutions. The different concentrations of the nanoparticle suspensions were obtained by dilution from a stock suspension, whose concentration was determined gravimetrically. A specific volume (1.5 mL) of the stock suspension was transferred to Eppendorf tubes previously weighted and centrifuged at 20,000 rpm for 3 h (Sorvall RC 26 Plus SA-300 rotor, DuPont). The excess of supernatant was then removed and the solid was dried overnight at 60 °C. The mass of the dried solid was determined using an analytical balance of high precision and the concentration of the suspension was calculated considering the volume that was pipetted, after subtracting the weight of the tube.

Antioxidant activity measurements were performed in duplicate at constant temperature (20 °C). For each lignin concentration, the radical scavenging reaction was monitored as a function of time by measuring the $DPPH^{\cdot}$ absorbance band at 515 nm (λ_{max}) in the beginning and after 16 and 30 min of reaction. Lignin nanoparticles in water (10 mg mL^{-1}) were blended (0.5, 3.0 and 10 wt.%) with neutral aqueous base cream (Dermavita ®) by mixing in a tube vortex stirrer (Phoenix AP 56). The UV–vis transmittance of lignin-based sunscreens was measured on a

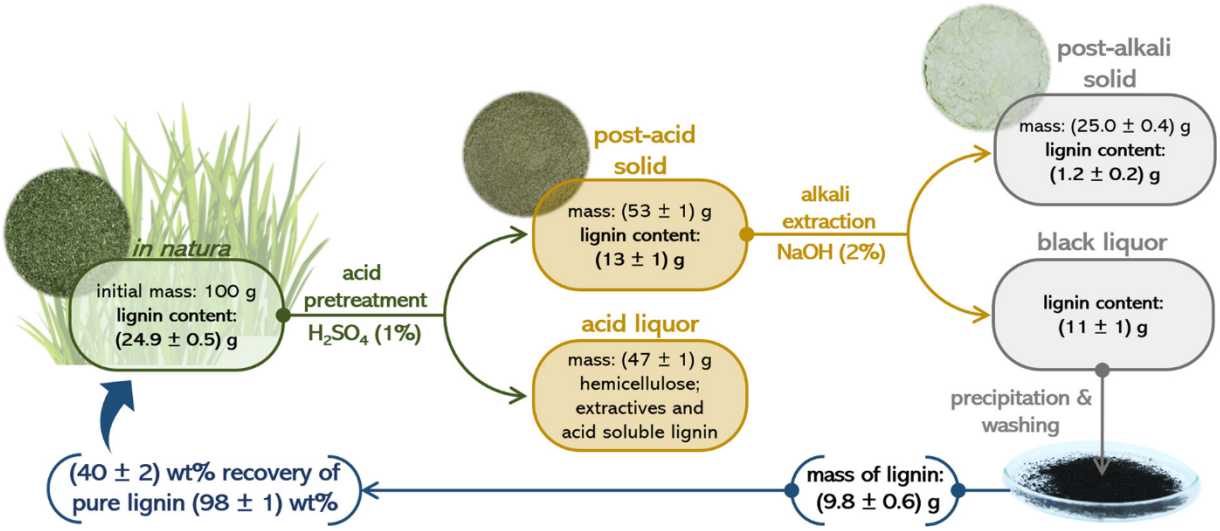

Fig. 2. Lignin contents in the elephant grass (*in natura*), in the solids recovered after each treatment step (post-acid and post-alkali) and the yield of recovered lignin. Contents are expressed on a dry weight basis as an average (± standard deviation) of triplicates.

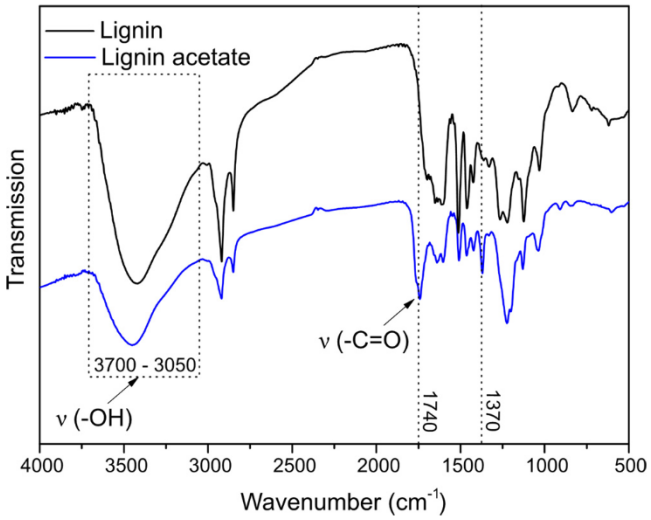

Fig. 3. FTIR spectra obtained for lignin isolated from elephant grass and for lignin after acetylation reaction (lignin acetate). The bands in 1740 cm^{-1} and 1370 cm^{-1} indicate the presence of the acetate group.

diffuse reflectance spectrometer (Shimadzu UV – 2450).

3. Results and discussion

3.1. Isolation and characterization of pure lignin from elephant grass using acid-alkali extraction

Delignification of elephant grass was carried out through two sequential treatments. In the first step, the biomass was hydrolysed with diluted sulfuric acid, leading to the removal of hemicellulose and extractives from the leaves mainly. Subsequently, the post-acid solid was treated with diluted NaOH leading to lignin solubilization in a black liquor, from which it could be precipitated in a succeeding step (Fig. 2). Fig. 2 shows the total mass recovered as solids or hydrolysates after each treatment step and the lignin content in the samples. The initial percentage of lignin in the leaves of elephant grass is (24.9 ± 0.5) wt. % and in the solid after the acid step it is (24.0 ± 2) wt. %. Considering that 47 % of the initial solid is hydrolysed in this acid step, ca. 52 wt. % of the initial lignin remains in the solid after the acid pretreatment. Following the two treatment steps, the final percentage of lignin in the substrate is only 5 %, showing an effective transfer of lignin from the solids to the black liquor.

Typically, the first acid pretreatment is able to remove 70 % of the hemicellulose and the total amount of extractives contained in elephant grass biomass (Nascimento and Rezende, 2018). The first acid pretreatment is thus important to allow a liquor purer in lignin to be obtained in the following alkali step. When lignin is extracted by alkaline treatments directly applied to the raw biomass, a high carbohydrate content (up to 30 %) is present, as observed by Nitsos et al. (2016) in lignin isolated from hardwoods and softwoods. Using the hemicellulose removing step, on the other hand, the final solid obtained here contains (98 ± 1) wt.% of lignin, as quantified by the NREL protocol (Sluiter et al., 2012; Nitsos et al., 2016). Moreover, residual sugars were not detected by liquid chromatography (HPLC) after hydrolysis of these lignin samples and their ash content was determined as (0.37 ± 0.07) % only. These results indicate that the washing and centrifuging cycles are important for purifying lignin and removing sugars and inorganic residues.

The evolution of the chemical composition in the solids after each hydrolysis step was also followed by solid state NMR-^{13}C (CPMAS), as presented in the supplementary material (Fig. S1 and Table S1). Solid state NMR spectra confirm that hemicellulose is removed, and lignin is kept in the solid after the first acid step, while almost all the lignin is extracted and transferred to the liquor after the second alkali step.

The acid-alkali treatment is thus an efficient method to extract lignin from elephant grass, since (40 ± 2) wt. % of the initial lignin content could be recovered as highly pure solid lignin. The lignin solubilised in the black liquor was recovered as precipitated lignin with a (85 ± 5) wt. % yield. These recovery yields are consistent with the values reported in the literature for wood pretreatments with NaOH solutions and higher than the yields typically reported for lignin extraction from sugarcane bagasse (5.5–13 wt.%) (Arni, 2018; Nitsos et al., 2016).

Two dimensional ^{13}C–^{1}H correlation HSQC NMR (Fig. S2 and Table S2) allowed the identification of syringyl, guaiacyl and *p*-hydroxyphenyl lignin units, as it is expected for grass lignins. In addition, it was also possible to identify the presence of β−O−4′ bonds, which is the predominant ether linkage type present in lignin (Upton and Kasko, 2016). It has been suggested in literature that the scission of β−O−4′ bonds is the main mechanism of lignin breaking down into smaller chains in chemical reactions catalysed by alkaline solutions (Fang and Smith, 2016). Henceforth, the presence of these arylglycerol-β-aryl linkages in the HSQC correlation spectrum indicates that the alkaline

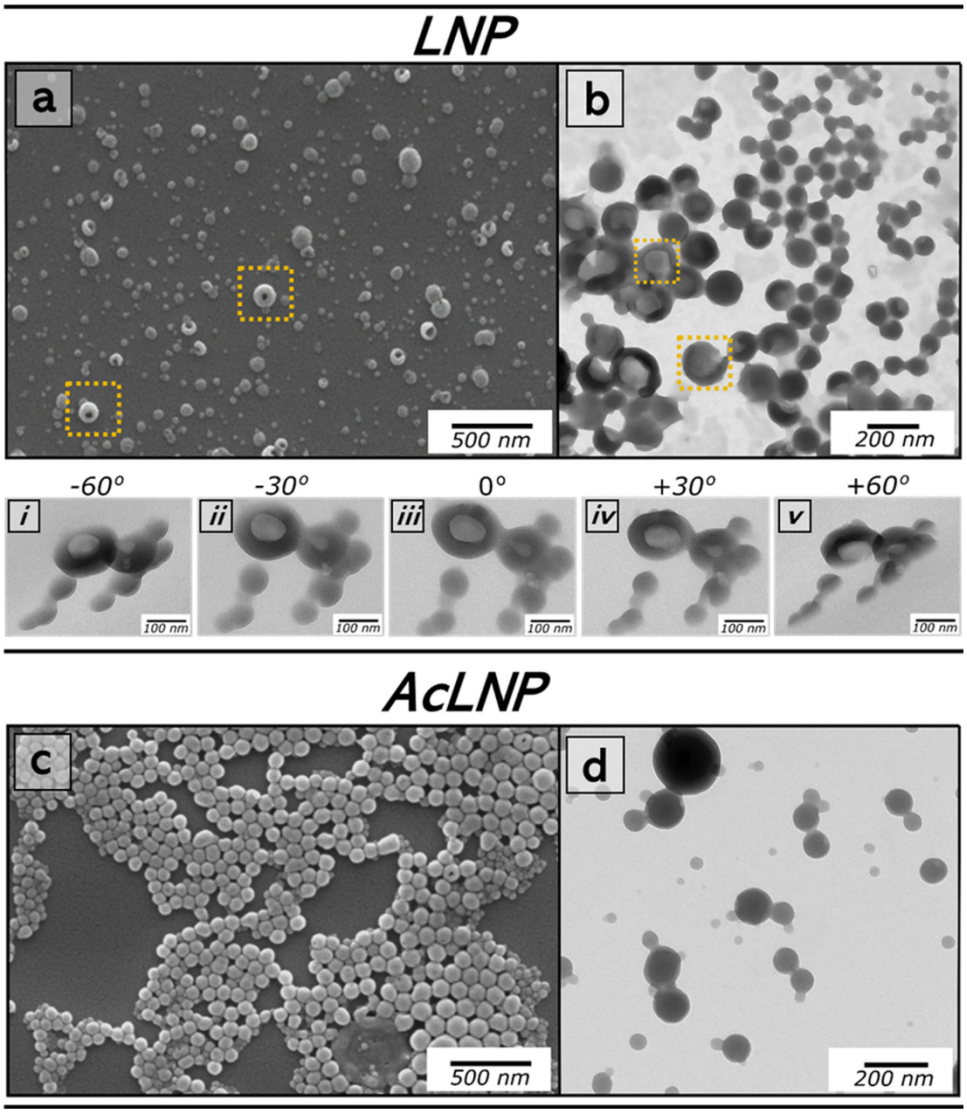

Fig. 4. a) and c) FESEM micrographies of lignin nanoparticles (*LNP*) and lignin acetate nanoparticles (*AcLNP*) both prepared by anti-solvent addition; b) and d) TEM micrographies of the respective nanoparticles. The sequence (i – v) shows the TEM angular series tilt from -60° to +60° to confirm the presence of hollow nanospheres (also indicated by the dash contour lines on FESEM and TEM micrographies). [Video on Supplementary Material].

treatment with NaOH 2 % (m/v) does not lead to a severe lignin fragmentation and lignin underwent little structural modification under the treatment conditions applied herewith.

Conversely, the cleavage of β−O−4′ bonds during the alkali treatment is fundamental for lignin antioxidant activity (Pan et al., 2006), which depends on the presence of phenolic hydroxyls. In addition, it was possible to identify an intense cross-peak signal for methoxyl groups that are found in guaiacyl and syringyl sub-units (Fig. S2). The quantitative ^{1}H NMR result for methoxyl content estimation corroborates the ^{13}C–^{1}H correlation result, since there is more methoxyl groups (*5.86 mmol* g^{-1} *of lignin*) than aliphatic (*4.90 mmol* g^{-1} *of lignin*) and phenolic (*3.85 mmol* g^{-1} *of lignin*) hydroxyl groups separately. Moreover, elephant grass lignin showed high concentration of phenolic hydroxyl groups in comparison to the contents typically reported in the literature (2.0 – 4.5 mmol g^{-1}) (Serrano et al., 2018).

Since the treatment did not lead to a severe lignin fragmentation, the isolated lignin has high molecular weights, as indicated by the high number-average (*Mn* $= 4730\,g\ mol^{-1}$) and weight-average (*Mw* $= 9180\,g\ mol^{-1}$) values. These values are somewhat consistent with results reported in literature for lignin recovered after soda pretreatments, with Mw between 800 and 15,000 g mol^{-1}, depending on the lignin biomass source (Kai et al., 2016). Notwithstanding, it is important to point up that GPC analysis was performed in a low polarity solvent (THF), which may promote aggregation of the amphiphilic macromolecule and result in high molecular weight value. Also, del Río et al. (2012) showed that milled wood lignins extracted from the cortex and the pith of elephant grass stems have molecular weights (M_w) in the range of 6920–6720 g mol^{-1} and a polydispersity value close to 3, which is higher than the polydispersity reported here (*1.94*) for lignin extracted from the leaves with the sequential acid-alkali treatment.

To evaluate the effect of hydroxyls present on the surface of the nanoparticles on their stability and antioxidant activity, lignin was acetylated and used to prepare lignin acetate nanoparticles. In Fig. 3, the spectra obtained for lignin isolated from elephant grass and for acetylated lignin can be compared.

The infrared spectra show that acetylation took place, as indicated by the increase of the FTIR bands in 1740 cm^{-1} (related to the (C═O) stretching in the acetyl group) and in 1370 cm^{-1} (related to the carbon-hydrogen (C–H) bending of CH_3 group). Additionally, the significant band intensity related to hydroxyl groups (3700 − 3050 cm^{-1}) indicates a partial acetylation. However, as exposed in the next sections, this partial acetylation is enough to track the influence of surface phenolic

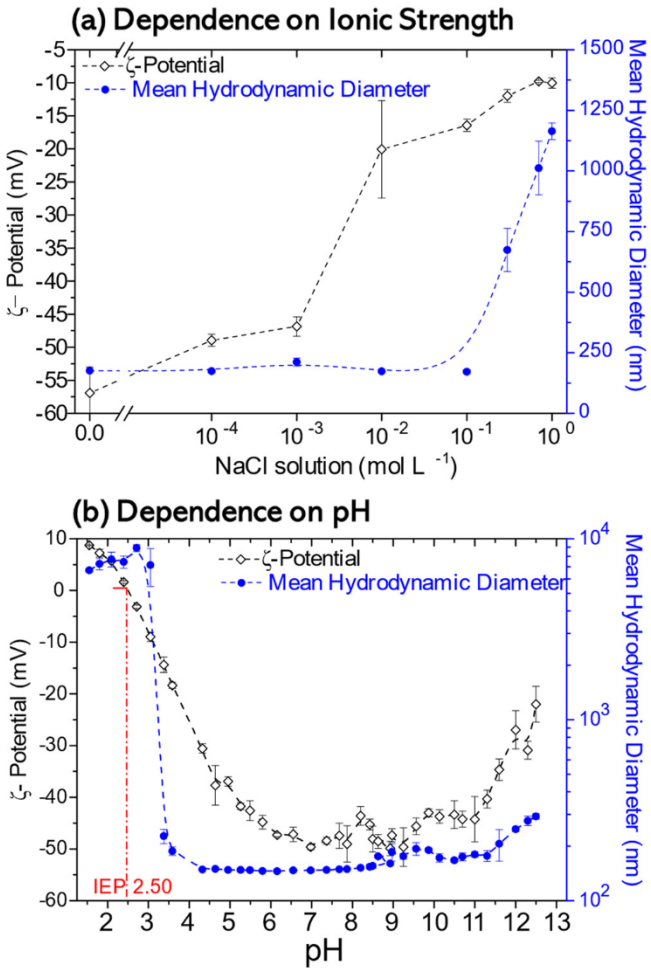

Fig. 5. Stability assay of lignin nanoparticles (*LNP*) under variable: a) ionic strength and b) pH. Nanoparticles showed isoelectric point (IEP) at 2.50 and are stable for NaCl concentrations below 0.01 mol L^{-1} and for pH ranges between 4 and 11 ($\zeta > 25$ mV). Error bars are standard deviation from triplicates.

hydroxyls on the stability and the antioxidant performance of lignin nanoparticles.

Qian et al.(2014) were the first to describe a method for lignin acetate nanoparticle preparation from lignin acetate synthesized with acetyl bromide, but this is an environmentally hazardous reagent. In contrast, our suspension of lignin acetate nanoparticles was prepared by a simpler method and the acetylation reaction was performed with acetic anhydride, which is less toxic than acetyl bromide. Albeit pyridine was used as solvent and catalyst for the acetylation of lignin, it can be still eco-friendly recovered by liquid-liquid extraction employing alkyl acetates (Kumar et al., 2011).

3.2. Lignin nanoparticles are prepared by self-assembling

Based on a simple method for lignin nanoparticle preparation (Richter et al., 2016), both lignin (*LNP*) and lignin acetate (*AcLNP*) nanoparticles could be assembled in a spherical shape (Fig. 4). Lignin nanoparticle preparation from lignin solubilized in acetone is a high yield process, with (93 ± 3) wt. % of the solubilized lignin being converted to non-acetylated nanoparticles (*LNP*) and (91 ± 5) wt. % to *AcLNP*. Considering the treatment losses (Fig. 2), (37 ± 3) wt. % and (36 ± 3) wt. % of the lignin contained in elephant grass *in natura* could be converted to *LNP* and *AcLNP*, respectively.

FESEM and TEM micrographies showed that some *LNP* – with diameter greater than 100 nm – also form hollow nanospheres with a single hole (as shown by the dash contour lines in Fig. 4). Additionally,

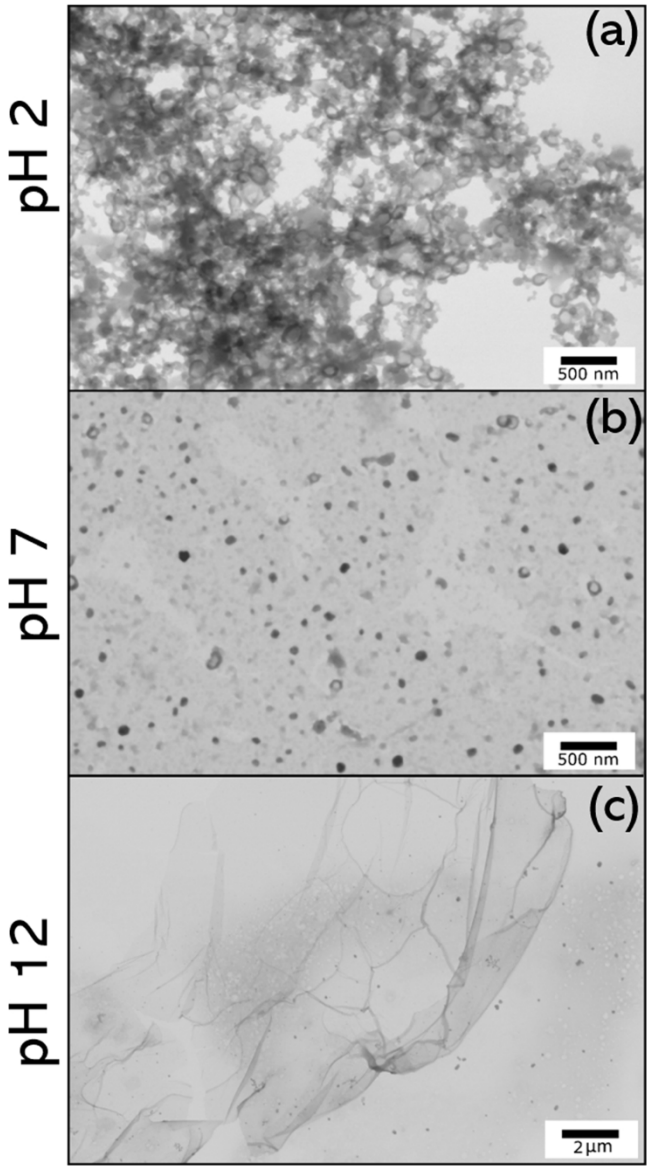

Fig. 6. STEM micrographies of LNP dispersed in water at different pH values a) 2; b) 7 and c) 12. The scale for micrography in c) is of 2 µm to emphasise the film formation.

results obtained by TEM angular series (Fig. 4, i–v) clearly proved that the lignin nanoparticles were hollow nanospheres and not toroids (lifebuoy shaped formats). In simple TEM images, these two morphologies appear to be the same, but the angular tilt during imaging allow their differentiation.

Since lignin nanoparticles are self-assembled by water pouring into the lignin solution, the question that rises here is: Why lignin aggregates are assembled into both nanoparticles and hollow nanospheres with single hole? The self-assembling process for lignin nanoparticles is somewhat simple to elucidate, once it is based on the strong tendency of water molecules to form H-bonds with each other – the so-called hydrophobic effect (Israelachvili, 2011). In this way, lignin molecules aggregate, increasing the aromatic π-π orbital interactions among each other and decreasing the overall interface area with water molecules (Rao et al., 2017). In this conformation, phenolic and carboxylic groups are displaced at the interface, as they are able to form effective H-bonds with water.

Conversely, the formation of hollow nanospheres is not as straightforwardly explained. In a recent work, Xiong et al. (2017)

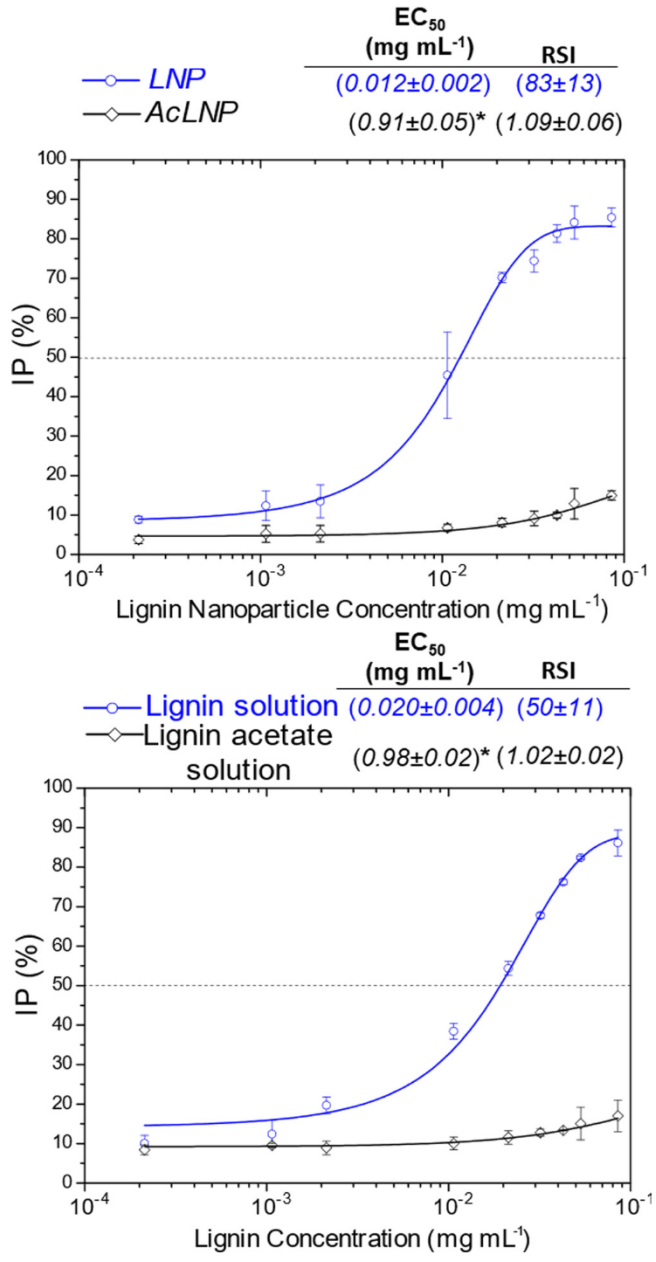

Fig. 7. Radical inhibition percentages (IP) for reaction time of 30 min as a function of the initial concentration of lignin/lignin acetate solutions and lignin nanoparticles (*LNP* and *AcLNP*) that reacted with the DPPH˙ radical. The data points were fitted by S SGompertz sigmoid function using OriginLab®. EC_{50} and RSI values are presented in the upper part of the figure. Error bars are standard deviation from duplicates. * Values were determined by extrapolation using the sigmoid fitting function.

explored the mechanism to assemble lignin hollow nanospheres using enzymatically hydrolysed lignin. They dissolved lignin in THF and induced nanosphere formation by water addition. According to their findings, the driving force to the assembling of hollow structures would be the effect of a small amount of impurities present in THF that led to phase separation between THF and water. However, the same explanation is not possible in the present work, since acetone is used as a solvent. Pure acetone is completely miscible with water and do not form a nanoemulsion system template as proposed in their work.

In our system, a plausible explanation is that vesicles are assembled during water addition as a consequence of the hydrophobic effect and to maximize π-π interactions between lignin aromatic hydrophobic blocks. Considering lignin amphiphilic character, the formation of vesicle-like structures would increase the density of intermolecular interactions between the hydrophilic blocks of lignin and water, in both inner and outer surfaces (Choucair et al., 2003; Israelachvili, 2011). The hollow spheres would then be formed with water evaporation during the preparation of samples for electron microscopy analysis. Another significant evidence to support this hypothesis is that *AcLNP* form fewer vesicle-like structures (Fig. 4c,d), since it has less hydroxyl groups on the surface (1.0 ± 0.2 mmol g^{-1}) in comparison to *LNP* (3.0 ± 1.0 mmol g^{-1}), as determined by conductometric titration (Table S3). Thus, for *AcLNP,* the increase of the particle size and the decrease of the surface-to-volume ratio does not impact considerably on the density of polar intermolecular interactions.

The size distribution of *LNP* and *AcLNP*, measured as the longest diameter of each particle in FESEM images (Fig. S3), shows that the average diameter was (*55 ± 26*) nm for *LNP* and (*86 ± 29*) nm for *AcLNP*. The occurrence of larger particles in lignin acetate is probably a consequence of the replacement of lignin hydroxyl groups by more hydrophobic carbonyl groups in acetylation. These carbonyls are able to establish π - π interactions with the lignin aromatic rings in the core of the nanoparticle, thus increasing the number of interacting chemical groups in the hydrophobic core and allowing the formation of more voluminous particles. Besides, the acetyl groups can both establish π-π interactions with aromatic rings in the core and form H-bonds with water on the surface, contrarily to the hydroxyls – that are necessarily placed on the surface.

Further, these particle sizes are considerably smaller than the average diameters reported in literature for lignin nanoparticle prepared by self-assembly (typically larger than 100 nm) (Lievonen et al., 2016; Qian et al., 2015a, 2014; Xiong et al., 2017). Besides this, both size distributions show that *LNP* and *AcLNP* are moderately disperse.

As shown in Fig. 5a, *LNP* dispersions were very stable in pure water with relatively high negative zeta potential, approximately −57 mV, inducing sufficient electrical double layer repulsion between the nanoparticles to avoid particle aggregation. In spite of this, by increasing the ionic strength up to 0.01, the nanoparticles begun to destabilize, as the zeta potential decreased to |-25 mV|, approximately (Morrison, 2002). This result shows that lignin nanoparticles should be stable in cream lotions with low salt concentration that are typically used for applications in dermocosmetic industries. *AcLNP* suspension is less stable than *LNP* suspension, with zeta potential of ca. − 40 mV, and it forms larger aggregates than *LNP* for ionic strength higher than 0.01 (Fig. S4); this result is due to the lower total concentration of ionizable groups on *AcLNP* surface in comparison to *LNP*, as the phenolic and carboxylic acid groups were acetylated.

As shown in Fig. 5b, by lowering the suspension pH, the zeta potential decreases (in modulus) progressively towards the point where it is zero (IEP at pH 2.50), and where the *LNP* suspensions lose their colloidal stability. As the pH decreases, the hydroxyls on the surface of the nanoparticles are successively protonated leading to insufficient electrical double layer repulsion and particle aggregation. Conversely, as the pH increases towards neutrality, the surface hydroxyls are progressively deprotonated and, also, more hydroxyls adsorb on the surface, turning the zeta potential more negative, and leading to a more stable nanoparticle suspension. Similar results were obtained for *AcLNP* (Fig. S4).

STEM results shown in Fig. 6a–c corroborate with the conclusions derived from the stability assay. It is possible to see nanoparticles agglomerated at pH 2, and particles well-defined and separated from each other at pH 7. Additionally, at pH 12, a film is observed in STEM measurements, probably due to the solubilisation of unstable nanoparticles in alkali medium, followed by drying during sample preparation. As a conclusion of ζ potential variation with pH, it is possible to infer that the lignin nanoparticles prepared here are stable and could be applied in cream lotions that typically have pH values from 5 to 7 (Lambers et al., 2006).

Table 1
Comparison of EC_{50} values of the elephant grass lignin and lignin nanoparticles obtained in the present work with other antioxidants and lignins reported in literature. RSI values were calculated (= $1/EC_{50}$) for comparison.

Sample	EC_{50} (mg mL^{-1})	RSI	Reference
Elephant grass lignin	0.020	50	In this work
Elephant grass lignin nanoparticles	0.012	83	In this work
Borassus flabellifer lignin	0.007	143	(Athinarayanan et al., 2018)
Hybrid poplar ethanol organosolv lignin	0.008	125	(Pan et al., 2006)
Alkali lignin after hydrogenolysis	0.025	40	(Zhao et al., 2018)
Rice straw alkali oxygen lignin*	0.025	40	(Jiang et al., 2018)
Alkali lignin from pulp mill	0.029	34	(Li et al., 2018)
Dewaxed palm oil acetosolv lignin	0.045	22	(de Menezes Nogueira et al., 2019)
Corn straw enzymatic hydrolysis lignin	0.066	15	(An et al., 2019)
Rice straw milled wood lignin*	0.070	14	(Jiang et al., 2018)
Corncob organosolv lignin	0.17	6	(Michelin et al., 2018)
Sugarcane bagasse lignin	0.38	3	(Kaur et al., 2017)
Other Antioxidants:			
Vitamin E	0.0037	263	(Pan et al., 2006)
BHT	0.038	26	(Li et al., 2018)
BHA	0.056	18	(Li et al., 2018)
Gallic acid	3.2	3	(Bekfelavi and Kuş, 2019)
Ascorbic acid	6.6	0.15	(Bekfelavi and Kuş, 2019)

* Approximate values.

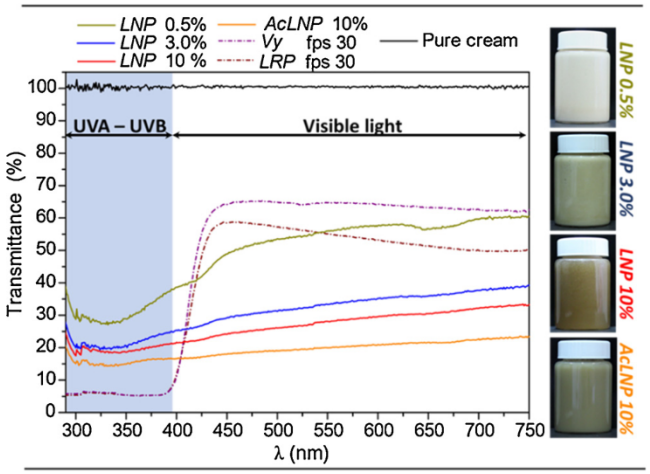

Fig. 8. UV–vis transmittance of neutral creams blended with *LNP* (0.5, 3.0 and 10 wt.%) and *AcLNP* (10 wt.%) in comparison to commercial sunscreens with fps 30 (LRP = La Roche-Posay® and Vy = Vichy Laboratories®). Visual aspect of the sunscreen lotions containing *LNP* and *AcLNP* on the right.

3.3. Lignin nanoparticles have higher antioxidant activity than lignin in solution

The antioxidant activity of lignin is strictly related to its chemical structure, as previously elucidated (Dizhbite et al., 2004). The colorimetric method used here to determine the antioxidant capacity is the most commonly used and based on the elimination of the π-radical ($DPPH^{\cdot}$). Several radical scavengers react with $DPPH^{\cdot}$ by delivering one electron and one proton, although, there might be different reaction mechanisms for $DPPH^{\cdot}$ scavenging (Fig. S5).

The method of Brand-Williams et al. (1995) was chosen to investigate the antioxidant capacity of lignin in solution and lignin nanoparticles. The results hereby are thus presented in terms of EC_{50}, which is defined as the amount of antioxidant required to reduce the initial concentration of the $DPPH^{\cdot}$ radical by 50 %, and in terms of the radical scavenging index (RSI), which is the inverse of EC_{50}. Thus, the lower the EC_{50} of an antioxidant, the higher is its RSI and its antioxidant efficiency. These parameters were obtained from the graphics of radical inhibition percentage as a function of the initial concentration of lignin/lignin acetate solutions and lignin nanoparticles (*LNP* and *AcLNP*) (Fig. 7) (Azadfar et al., 2015; Pan et al., 2006). Two different reaction times were evaluated (16 and 30 min), but there is no significant difference between them in terms of RSIs (Table S4 and Fig. S6).

According to Fig. 7, both lignin in solution and *LNP* have higher radical inhibition percentages than lignin acetate in solution and *AcLNP* since, for the later ones, the amount of phenolic hydroxyls available to react with the $DPPH^{\cdot}$ radical was reduced. Moreover, this experimental observation confirms that the antioxidant activity of *LNP* is related to the presence of phenolic groups on the surface of the nanoparticle.

Surprisingly, *LNP* showed lower EC_{50} concentrations and, consequently, higher RSI values than lignin in solution. A possible explanation for this result is that, lignin in solution is organized in a such way as to maximize the number of intermolecular interactions with other lignin macromolecules and with the solvent. Consequently, its aromatic hydroxyls are not easily accessed by the $DPPH^{\cdot}$ radical – as compared to the phenolic hydroxyls that are oriented on the surface of the nanoparticles. This result is even more important, considering that lignin solutions (in organic and alkaline solvents) are not applicable in dermocosmetics, while lignin nanoparticles dispersed in water would be very useful for this purpose.

Among the synthetic antioxidants most used in the food and dermocosmetics industries, butylhydroxytoluene (BHT) and butylated hydroxyanisole (BHA) have a less efficient EC_{50} in comparison to *LNP* (Table 1) (Li et al., 2018). By comparing the EC_{50} and RSI values obtained for lignin in solution with values reported in the literature (Table 1), it was possible to conclude that the lignin extracted from elephant grass leaves has high antioxidant activity in comparison to many previously reported lignins. In a recent work, Kaur et al.(2017) found a RSI value of 2.63 for lignin in solution extracted from sugarcane bagasse through NaOH treatment, which is considerably smaller than the RSI for elephant grass lignin in solution (RSI = 50).

3.4. Lignin nanoparticles for tinted sunscreens

The high radical scavenging ability of lignin nanoparticles reported here can be coupled with its UV–vis light blocking capability. Some few works have reported the potential of using lignin in sunscreens, forasmuch as cytotoxicity tests have certified that it is safe (Qian et al., 2015b; Wang et al., 2019). Furthermore, recent studies point that sun protection should also include shielding against visible radiation, as visible light coupled with UVA radiation causes deleterious effects on skin (Tonolli et al., 2017). Here, lignin nanoparticles (*LNP* and *AcLNP*) were blended with a neutral aqueous base cream and the UV–vis

transmittance measurements in Fig. 8 show that the blended creams with *LNP* (3.0 and 10 wt.%) and *AcLNP* (10 wt.%) have lower transmittance in visible region in comparison to commercial sunscreens with fps 30. Moreover, as shown in Fig. 8 the visual aspect of the sunscreen lotions prepared with *LNP* and *AcLNP* concentrations within 0.5–10% look similar to tinted creams.

In addition, by increasing the percentage of *LNP* in the cream, the performance towards UV–vis light shielding was enhanced. As expected, the cream with 10 wt. % of *AcLNP* showed better UV–vis light screening, since the acetate is an additional absorbing functional group (Qian et al., 2015b). In view of the present concerns related with the negative impact of sunscreen formulations in the marine biota, sunscreens based on the photoabsorption of lignin nanoparticles could be an environmentally friendly alternative to the commercial ones, thus reducing the environmental impacts in coral reefs (Singer et al., 2019).

4. Conclusions

Pure lignin could be fractionated here from elephant grass by a simple and greener double-step acid-alkali treatment, in a process that did not lead to severe lignin fragmentation and allowed sufficient cleavage of β-O-4 ether bonds, creating free phenolic hydroxyl groups. Spherical lignin nanoparticles, stable under a broad pH range (5–11) and under ionic strengths lower than 0.01, were prepared from this lignin. These nanoparticles are especially indicated for applications in cream lotions and tinted sunscreens due to lignin biocompatibility and biodegradability, great UV–vis absorption, and antioxidant activity (RSI ca. 83) higher than the ones typically reported for the commercial antioxidants BHT and BHA.

Funding

This research project was funded by FAPESP (grants #2018/23769-1 and 2016/13602-7), and CNPq (grant #420031/2018-9). This study was financed in part by the Coordenação de Aperfeiçoamento de Pessoal de Nível Superior - Brasil (CAPES) - Finance Code 001.

CRediT authorship contribution statement

Henrique Trevisan: Conceptualization, Methodology, Validation, Formal analysis, Investigation, Writing - original draft, Writing - review & editing, Visualization. **Camila A. Rezende:** Conceptualization, Resources, Writing - original draft, Writing - review & editing, Supervision, Project administration, Funding acquisition.

Declaration of Competing Interest

There are no conflicts to declare.

Acknowledgements

We express our gratitude to INOMAT and Dr. Douglas S. Silva for technical support during TEM work.

Appendix A. Supplementary data

Supplementary material related to this article can be found, in the online version, at doi:https://doi.org/10.1016/j.indcrop.2020.112105.

References

Ahvazi, B., Cloutier, É., Wojciechowicz, O., Ngo, T.-D., 2016. Lignin profiling: a guide for selecting appropriate lignins as precursors in biomaterials development. ACS Sustain. Chem. Eng. 4, 5090–5105. https://doi.org/10.1021/acssuschemeng.6b00873.

Alonso, C., Martí, M., Martínez, V., Rubio, L., Parra, J.L., Coderch, L., 2013. Antioxidant cosmeto-textiles: skin assessment. Eur. J. Pharm. Biopharm. 84, 192–199. https://doi.org/10.1016/j.ejpb.2012.12.004.

Amorati, R., Foti, M.C., Valgimigli, L., 2013. Antioxidant activity of essential oils. J. Agric. Food Chem. 61, 10835–10847. https://doi.org/10.1021/jf403496k.

An, L., Si, C., Wang, G., Sui, W., Tao, Z., 2019. Enhancing the solubility and antioxidant activity of high-molecular-weight lignin by moderate depolymerization via in situ ethanol/acid catalysis. Ind. Crops Prod. 128, 177–185. https://doi.org/10.1016/j.indcrop.2018.11.009.

Arni, S.A., 2018. Extraction and isolation methods for lignin separation from sugarcane bagasse: a review. Ind. Crops Prod. 115, 330–339. https://doi.org/10.1016/j.indcrop.2018.02.012.

Athinarayanan, J., Periasamy, V.S., Qasem, A.A., Alshatwi, A.A., 2018. Borassus flabellifer biomass lignin: isolation and characterization of its antioxidant and cytotoxic properties. Sustain. Chem. Pharm. 10, 89–96. https://doi.org/10.1016/j.scp.2018.10.001.

Azadfar, M., Gao, A.H., Bule, M.V., Chen, S., 2015. Structural characterization of lignin: a potential source of antioxidants guaiacol and 4-vinylguaiacol. Int. J. Biol. Macromol. 75, 58–66. https://doi.org/10.1016/j.ijbiomac.2014.12.049.

Bekfelavi, E.Y., Kuş, N.Ş., 2019. The synthesis of monocyclic and bicyclic molecules and their antioxidant properties. J. Mol. Struct. 1189, 249–256. https://doi.org/10.1016/j.molstruc.2019.04.034.

Brand-Williams, W., Cuvelier, M.E., Berset, C., 1995. Use of a free radical method to evaluate antioxidant activity. Lwt - Food Sci. Technol. 28, 25–30. https://doi.org/10.1016/S0023-6438(95)80008-5.

Choucair, A.A., Kycia, A.H., Eisenberg, A., 2003. Kinetics of Fusion of Polystyrene- *b* -poly (acrylic acid) Vesicles in Solution. Langmuir 19, 1001–1008. https://doi.org/10.1021/la026187k.

de Menezes Nogueira, I., Avelino, F., de Oliveira, D.R., Souza, N.F., Rosa, M.F., Mazzetto, S.E., Lomonaco, D., 2019. Organic solvent fractionation of acetosolv palm oil lignin: the role of its structure on the antioxidant activity. Int. J. Biol. Macromol. 122, 1163–1172. https://doi.org/10.1016/j.ijbiomac.2018.09.066.

del Río, J.C., Prinsen, P., Rencoret, J., Nieto, L., Jiménez-Barbero, J., Ralph, J., Martínez, Á.T., Gutiérrez, A., 2012. Structural characterization of the lignin in the cortex and pith of elephant grass (*Pennisetum purpureum*) stems. J. Agric. Food Chem. 60, 3619–3634. https://doi.org/10.1021/jf300099g.

Dizhbite, T., Telysheva, G., Jurkjane, V., Viesturs, U., 2004. Characterization of the radical scavenging activity of lignins natural antioxidants. Bioresour. Technol. 95, 309–317. https://doi.org/10.1016/j.biortech.2004.02.024.

Duan, H., Wang, D., Li, Y., 2015. Green chemistry for nanoparticle synthesis. Chem. Soc. Rev. 44, 5778–5792. https://doi.org/10.1039/C4CS00363B.

Fang, Z., Smith, R.L., 2016. Production of biofuels and chemicals from lignin. Biofuels and Biorefineries 6, 3–24. https://doi.org/10.1007/978-981-10-1965-4. Springer, 2016. ISBN 978-981-10-1964-7.

Figueiredo, P., Lintinen, K., Hirvonen, J.T., Kostiainen, M.A., Santos, H.A., 2018. Properties and chemical modifications of lignin: towards lignin-based nanomaterials for biomedical applications. Prog. Mater. Sci. 93, 233–269. https://doi.org/10.1016/j.pmatsci.2017.12.001.

Florian, T.D.M., Villani, N., Aguedo, M., Jacquet, N., Thomas, H.G., Gerin, P., Magali, D., Richel, A., 2019. Chemical composition analysis and structural features of banana rachis lignin extracted by two organosolv methods. Ind. Crops Prod. 132, 269–274. https://doi.org/10.1016/j.indcrop.2019.02.022.

Froass, P.M., Ragauskas, A.J., Jiang, J.E., 1998. NMR studies part 3: analysis of lignins from modern kraft pulping technologies. Holzforschung 52, 385–390. https://doi.org/10.1515/hfsg.1998.52.4.385.

Guo, G., Chen, W., Chen, W., Men, L., Hwang, W., 2008. Characterization of dilute acid pretreatment of silvergrass for ethanol production. Bioresour. Technol. 99, 6046–6053. https://doi.org/10.1016/j.biortech.2007.12.047.

Hu, G., Cateto, C., Pu, Y., Samuel, R., Ragauskas, A.J., 2012. Structural characterization of switchgrass lignin after ethanol organosolv pretreatment. Energy Fuels 26, 740–745. https://doi.org/10.1021/ef201477p.

Israelachvili, J.N., 2011. Intermolecular and Surface Forces, 3rd ed. Elsevier, California, USA.

Jeong, E., Im, W.-T., Kim, D.-H., Kim, M.-S., Kang, S., Shin, H.-S., Chae, S.-R., 2014. Different susceptibilities of bacterial community to silver nanoparticles in wastewater treatment systems. Journal of Environmental Science and Health, Part A 49, 685–693. https://doi.org/10.1080/10934529.2014.865454.

Jiang, B., Zhang, Y., Gu, L., Wu, W., Zhao, H., Jin, Y., 2018. Structural elucidation and antioxidant activity of lignin isolated from rice straw and alkali-oxygen black liquor. Int. J. Biol. Macromol. 116, 513–519. https://doi.org/10.1016/j.ijbiomac.2018.05.063.

Kai, D., Tan, M.J., Chee, P.L., Chua, Y.K., Yap, Y.L., Loh, X.J., 2016. Towards lignin-based functional materials in a sustainable world. Green Chem. 18, 1175–1200. https://doi.org/10.1039/C5GC02616D.

Kaur, R., Uppal, S.K., Sharma, P., 2017. Antioxidant and antibacterial activities of sugarcane bagasse lignin and chemically modified lignins. Sugar Tech 19, 675–680. https://doi.org/10.1007/s12355-017-0513-y.

M. Kumar, S.K. Dixit, S.K. Singh, A. Agarwal, US Pat., 8,057,643 B2, 2011; JUBILANT ORGQANOSYS LIMITED.

Lambers, H., Piessens, S., Bloem, A., Pronk, H., Finkel, P., 2006. Natural skin surface pH is on average below 5, which is beneficial for its resident flora. Int. J. Cosmet. Sci. 28, 359–370. https://doi.org/10.1111/j.1467-2494.2006.00344.x.

Li, Z., Zhang, J., Qin, L., Ge, Y., 2018. Enhancing antioxidant performance of lignin by enzymatic treatment with laccase. ACS Sustain. Chem. Eng. 6, 2591–2595. https://doi.org/10.1021/acssuschemeng.7b04070.

Lievonen, M., Valle-Delgado, J.J., Mattinen, M.-L., Hult, E.-L., Lintinen, K., Kostiainen, M.A., Paananen, A., Szilvay, G.R., Setälä, H., Österberg, M., 2016. A simple process for lignin nanoparticle preparation. Green Chem. 18, 1416–1422. https://doi.org/10.1039/C5GC01436K.

Lima, M.A., Gomez, L.D., Steele-King, C.G., Simister, R., Bernardinelli, O.D., Carvalho, M.A., Rezende, C.A., Labate, C.A., McQueen-Mason, S.J., Polikarpov, I., 2014. Evaluating the composition and processing potential of novel sources of Brazilian biomass for sustainable biorenewables production. Biotechnol. Biofuels 7, 10. https://doi.org/10.1186/1754-6834-7-10.

Menegol, D., Scholl, A.L., Dillon, A.J.P., Camassola, M., 2017. Use of elephant grass (Pennisetum purpureum) as substrate for cellulase and xylanase production in solid-state cultivation by Penicillium echinulatum. Braz. J. Chem. Eng. 34, 691–700. https://doi.org/10.1590/0104-6632.20170343s20150822.

Michelin, M., Liebentritt, S., Vicente, A.A., Teixeira, J.A., 2018. Lignin from an integrated process consisting of liquid hot water and ethanol organosolv: physicochemical and antioxidant properties. Int. J. Biol. Macromol. 120, 159–169. https://doi.org/10.1016/j.ijbiomac.2018.08.046.

Moreira-Vilar, F.C., Siqueira-Soares, R., de, C., Finger-Teixeira, A., de Oliveira, D.M., Ferro, A.P., 2014. The acetyl bromide method is faster, simpler and presents best recovery of lignin in different herbaceous tissues than Klason and thioglycolic acid methods. PLoS One 9 (10), e110000. https://doi.org/10.1371/journal.pone.0110000.

Morrison, Ian D.S.R., 2002. Colloidal Dispersions. Suspensions, Emulsions and Foams. Wiley-Interscience, New York.

Nascimento, S.A., Rezende, C.A., 2018. Combined approaches to obtain cellulose nanocrystals, nanofibrils and fermentable sugars from elephant grass. Carbohydr. Polym. 180, 38–45. https://doi.org/10.1016/j.carbpol.2017.09.099.

Nitsos, C., Stoklosa, R., Karnaouri, A., Vörös, D., Lange, H., Hodge, D., Crestini, C., Rova, U., Christakopoulos, P., 2016. Isolation and characterization of organosolv and alkaline lignins from hardwood and softwood biomass. ACS Sustain. Chem. Eng. 4, 5181–5193. https://doi.org/10.1021/acssuschemeng.6b01205.

Pan, X., Kadla, J.F., Ehara, K., Gilkes, N., Saddler, J.N., 2006. Organosolv ethanol lignin from hybrid poplar as a radical scavenger: relationship between lignin structure, extraction conditions, and antioxidant activity. J. Agric. Food Chem. 54, 5806–5813. https://doi.org/10.1021/jf0605392.

Qian, Y., Deng, Y., Qiu, X., Li, H., Yang, D., 2014. Formation of uniform colloidal spheres from lignin, a renewable resource recovered from pulping spent liquor. Green Chem. 16, 2156. https://doi.org/10.1039/c3gc42131g.

Qian, Y., Qiu, X., Zhong, X., Zhang, D., Deng, Y., Yang, D., Zhu, S., 2015a. Lignin reverse micelles for UV-Absorbing and high mechanical performance thermoplastics. Ind. Eng. Chem. Res. 54, 12025–12030. https://doi.org/10.1021/acs.iecr.5b03360.

Qian, Y., Qiu, X., Zhu, S., 2015b. Lignin: a nature-inspired sun blocker for broad-spectrum sunscreens. Green Chem. 17, 320–324. https://doi.org/10.1039/C4GC01333F.

Ragauskas, A.J., Beckham, G.T., Biddy, M.J., Chandra, R., Chen, F., Davis, M.F., Davison, B.H., Dixon, R.A., Gilna, P., Keller, M., Langan, P., Naskar, A.K., Saddler, J.N., Tschaplinski, T.J., Tuskan, G.A., Wyman, C.E., 2014. Lignin valorization: improving lignin processing in the biorefinery. Science 344, 1246843. https://doi.org/10.1126/science.1246843.

Rao, X., Liu, Yongzhuang, Zhang, Q., Chen, W., Liu, Yixing, Yu, H., 2017. Assembly of Organosolv Lignin Residues into Submicron Spheres: The Effects of Granulating in Ethanol/Water Mixtures and Homogenization. ACS Omega 2, 2858–2865. https://doi.org/10.1021/acsomega.7b00285.

Rezende, C.A., de Lima, M.A., Maziero, P., deAzevedo, E.R., Garcia, W., Polikarpov, I., 2011. Chemical and morphological characterization of sugarcane bagasse submitted to a delignification process for enhanced enzymatic digestibility. Biotechnol. Biofuels 4 (1), 54. https://doi.org/10.1186/1754-6834-4-54.

Rezende, C.A., Atta, B.W., Breitkreitz, M.C., Simister, R., Gomez, L.D., McQueen-Mason, S.J., 2018. Optimization of biomass pretreatments using fractional factorial experimental design. Biotechnol. Biofuels 11, 206. https://doi.org/10.1186/s13068-018-1200-2.

Richter, A.P., Bharti, B., Armstrong, H.B., Brown, J.S., Plemmons, D., Paunov, V.N., Stoyanov, S.D., Velev, O.D., 2016. Synthesis and Characterization of Biodegradable Lignin Nanoparticles with Tunable Surface Properties. Langmuir 32, 6468–6477. https://doi.org/10.1021/acs.langmuir.6b01088.

Romdhane, A., Aurousseau, M., Guillet, A., Mauret, E., 2015. Effect of pH and ionic strength on the electrical charge and particle size distribution of starch nanocrystal suspensions. Starch - Stärke 67, 319–327. https://doi.org/10.1002/star.201400181.

Schutyser, W., Renders, T., Van den Bosch, S., Koelewijn, S.-F., Beckham, G.T., Sels, B.F., 2018. Chemicals from lignin: an interplay of lignocellulose fractionation, depolymerisation, and upgrading. Chem. Soc. Rev. 47, 852–908. https://doi.org/10.1039/C7CS00566K.

Serrano, L., Esakkimuthu, E.S., Marlin, N., Brochier-Salon, M.-C., Mortha, G., Bertaud, F., 2018. Fast, Easy, and Economical Quantification of Lignin Phenolic Hydroxyl Groups: Comparison with Classical Techniques. Energy Fuels 32, 5969–5977. https://doi.org/10.1021/acs.energyfuels.8b00383.

Singer, S., Karrer, S., Berneburg, M., 2019. Modern sun protection. Curr. Opin. Pharmacol. 46, 24–28. https://doi.org/10.1016/j.coph.2018.12.006.

Sluiter, A., Hames, B., Ruiz, R., Scarlata, C., Sluiter, J., Templeton, D., Crocker, D., 2012. NREL/TP-510-42618. Determination of Structural Carbohydrates and Lignin in Biomass.

Somerville, C., Youngs, H., Taylor, C., Davis, S.C., Long, S.P., 2010. Feedstocks for lignocellulosic biofuels. Science 329, 790–792. https://doi.org/10.1126/science.1189268.

Strassberger, Z., Tanase, S., Rothenberg, G., 2014. The pros and cons of lignin valorisation in an integrated biorefinery. RSC Adv. 4, 25310–25318. https://doi.org/10.1039/C4RA04747H.

Tolbert, A., Akinosho, H., Khunsupat, R., Naskar, A.K., Ragauskas, A.J., 2014. Characterization and analysis of the molecular weight of lignin for biorefining studies. Biofuels Bioprod. Biorefining 8, 836–856. https://doi.org/10.1002/bbb.1500.

Tonolli, P.N., Chiarelli-Neto, O., Santacruz-Perez, C., Junqueira, H.C., Watanabe, I.-S., Ravagnani, F.G., Martins, W.K., Baptista, M.S., 2017. Lipofuscin generated by UVA turns keratinocytes photosensitive to visible light. J. Invest. Dermatol. 137, 2447–2450. https://doi.org/10.1016/j.jid.2017.06.018.

Upton, B.M., Kasko, A.M., 2016. Strategies for the conversion of lignin to high-value polymeric materials: review and perspective. Chem. Rev. 116, 2275–2306. https://doi.org/10.1021/acs.chemrev.5b00345.

Valgimigli, L., Baschieri, A., Amorati, R., 2018. Antioxidant activity of nanomaterials. J. Mater. Chem. B 6, 2036–2051. https://doi.org/10.1039/C8TB00107C.

Wang, B., Sun, D., Wang, H.-M., Yuan, T.-Q., Sun, R.-C., 2019. Green and facile preparation of regular lignin nanoparticles with high yield and their natural broad-spectrum sunscreens. ACS Sustain. Chem. Eng. 7, 2658–2666. https://doi.org/10.1021/acssuschemeng.8b05735.

Xiong, F., Han, Y., Wang, S., Li, G., Qin, T., Chen, Y., Chu, F., 2017. Preparation and formation mechanism of renewable lignin hollow nanospheres with a single hole by self-assembly. ACS Sustain. Chem. Eng. 5, 2273–2281. https://doi.org/10.1021/acssuschemeng.6b02585.

Yang, W., Fortunati, E., Bertoglio, F., Owczarek, J.S., Bruni, G., Kozanecki, M., Kenny, J.M., Torre, L., Visai, L., Puglia, D., 2018. Polyvinyl alcohol/chitosan hydrogels with enhanced antioxidant and antibacterial properties induced by lignin nanoparticles. Carbohydr. Polym. 181, 275–284. https://doi.org/10.1016/j.carbpol.2017.10.084.

Yang, W., Fortunati, E., Gao, D., Balestra, G.M., Giovanale, G., He, X., Torre, L., Kenny, J.M., Puglia, D., 2018a. Valorization of acid isolated high yield lignin nanoparticles as innovative Antioxidant/Antimicrobial organic materials. ACS Sustain. Chem. Eng. 6, 3502–3514. https://doi.org/10.1021/acssuschemeng.7b03782.

Yang, W., Rallini, M., Wang, D.-Y., Gao, D., Dominici, F., Torre, L., Kenny, J.M., Puglia, D., 2018b. Role of lignin nanoparticles in UV resistance, thermal and mechanical performance of PMMA nanocomposites prepared by a combined free-radical graft polymerization/masterbatch procedure. Compos. Part A Appl. Sci. Manuf. 107, 61–69. https://doi.org/10.1016/j.compositesa.2017.12.030.

Yang, W., Owczarek, J.S., Fortunati, E., Kozanecki, M., Mazzaglia, A., Balestra, G.M., Kenny, J.M., Torre, L., Puglia, D., 2016. Antioxidant and antibacterial lignin nanoparticles in polyvinyl alcohol/chitosan films for active packaging. Ind. Crops Prod. 94, 800–811. https://doi.org/10.1016/j.indcrop.2016.09.061.

Zhao, L., Ouyang, X., Ma, G., Qian, Y., Qiu, X., Ruan, T., 2018. Improving antioxidant activity of lignin by hydrogenolysis. Ind. Crops Prod. 125, 228–235. https://doi.org/10.1016/j.indcrop.2018.09.002.

Zhao, W., Simmons, B., Singh, S., Ragauskas, A., Cheng, G., 2016. From lignin association to nano-/micro-particle preparation: extracting higher value of lignin. Green Chem. 18, 5693–5700. https://doi.org/10.1039/C6GC01813K.